Synthesis of $BaTiO_3$ Core−Shell Particles and Fabrication of Dielectric Ceramics with Local Graded Structure

Maria Teresa Buscaglia,[†] Massimo Viviani,[†] Zhe Zhao,[‡] Vincenzo Buscaglia,*[,†] and Paolo Nanni[§]

Institute for Energetics and Interphases, National Research Council, via De Marini 6, I-16149 Genoa, Italy, Department of Inorganic Chemistry, University of Stockholm, S106 91 Stockholm, Sweden, and Department of Process and Chemical Engineering, University of Genoa, P. le Kennedy, Fiera del Mare, Pad. D, I-16129 Genoa, Italy

Received February 17, 2006. Revised Manuscript Received June 15, 2006

The coating of $BaTiO_3$ particles with a different perovskite and the subsequent consolidation to dense ceramics retaining a radial composition gradient within the single grains are presented and discussed. A shell of $SrTiO_3$ or $BaZrO_3$ was directly grown on the surface of $BaTiO_3$ spherical templates suspended in aqueous solution by means of a precipitation process making use of inorganic precursors. The overall composition and the particle size can be tailored over a wide range. Densification of the resulting core−shell particles was realized using spark plasma sintering or conventional sintering. Dense ceramics with locally graded structure can be only obtained by a careful choice of the sintering conditions, that is, controlling the interdiffusion between core and shell. The final materials show strongly modified dielectric properties in comparison to both the parent compounds and the homogeneous solid solutions. The proposed approach is generic and suggests a new avenue to create functional and structural polycrystalline materials with locally graded structure by the controlled sintering of core−shell particles.

1. Introduction

A significant modification of the properties of functional materials can be obtained by generating periodic chemical composition fluctuations on the local scale. A good example is provided by ferroelectric ceramic oxides, such as polycrystalline $BaTiO_3$, extensively used in the electronic industry as dielectrics in multilayer ceramic capacitors (MLCCs) and other components because of its high relative dielectric constant and the low losses.[1] In the field of high-permittivity dielectrics it is highly desirable to have the grains of the ceramic composed of a core of virtually pure $BaTiO_3$ surrounded by a shell where Ti is partially replaced by a different element, like Zr or Nb. The local gradient gives a distribution of the Curie temperature (T_C) and, consequently, flatter dielectric temperature characteristics in comparison to pure $BaTiO_3$.[2−5] These locally inhomogeneous ceramics are usually obtained by mixing a $BaTiO_3$ powder with a second oxide, like ZrO_2 or Nb_2O_5, and then sintering in the presence of a liquid phase. In such a condition densification is accompanied by recrystallization and partial interdiffusion, resulting in grains with core−shell structure. Dielectric materials of this kind have found extensive application in the fabrication of MLCCs. However, final microstructure and grain size are not easily controlled; moreover, the method is not generic, and each system has to be empirically optimized.

In recent years there has been an increasing interest in the fabrication of colloidal core−shell materials.[6−12] The modification of fine particles by coating with inorganic materials of different composition has been extensively studied to change their interfacial characteristics (for instance, making them dispersable in a liquid or glassy phase)[13−15] as well as their optical, magnetic, catalytic, and thermal properties.[16−24] In principle, colloidal core−shell particles

* Corresponding author. E-mail: v.buscaglia@ge.ieni.cnr.it.
† National Research Council.
‡ University of Stockholm.
§ University of Genoa.

(1) Reynolds, T. G., III. *Am. Ceram. Soc. Bull.* **2001**, *80*, 29.
(2) Kahn, M. *J. Am. Ceram. Soc.* **1971**, *54*, 455,
(3) Hennings, D.; Rosenstein, G. *J. Am. Ceram. Soc.* **1984**, *67*, 249.
(4) Armstrong, T. R.; Morgens, L. E.; Maurice, A. K.; Buchanan, R. C. *J. Am. Ceram. Soc.* **1989**, *72*, 605.
(5) Armstrong, T. R.; Young, K. A.; Buchanan, R. C. *J. Am. Ceram. Soc.* **1990**, *73*, 700.
(6) Caruso, F. *Adv. Mater.* **2001**, *13*, 11.
(7) Caruso, R. A.; Antonietti, M. *Chem. Mater.* **2001**, *13*, 3272.
(8) Walsh, D.; Mann, S. *Nature* **1995**, *377*, 320.
(9) Caruso, F.; Caruso, R. A.; Möhwald, H. *Science* **1998**, *282*, 1111.
(10) Jiang, P.; Bertone, J. F.; Colvin, V. L. *Science* **2001**, *291*, 453.
(11) Lauhon, L. J.; Gudiksen, M. S.; Wang, D.; Lieber, C. M. *Nature* **2002**, *420*, 57.
(12) Radt, B.; Smith, T. A.; Caruso, F. *Adv. Mater.* **2004**, *16*, 2184.
(13) Philipse, A. P.; van Bruggen, M. P. B.; Pathmamanoharan, C. *Langmuir* **1994**, *10*, 92.
(14) Liz-Marzán, L. M.; Giersig, M.; Mulvaney, P. *Langmuir* **1996**, *12*, 4329.
(15) (a) Ohmori, M.; Matijevic, E. *J. Colloid Interface Sci* **1993**, *160*, 288. (b) Hardikar, V. V.; Matijevic, E. *J. Colloid Interface Sci.* **2000**, *221*, 133.
(16) Ocaña, M.; Hsu, W. P.; Matijevic, E. *Langmuir* **1991**, *7*, 2911.
(17) Hsu, W. P.; Yu, R. C.; Matijevic, E. *J. Colloid Interface Sci.* **1993**, *156*, 56.
(18) Aliev, F. G.; Correa-Duarte, M. A.; Mamedov, A.; Ostrander, J. W.; Giersig, M.; Liz-Marzán, L. M.; Kotov, N. A. *Adv. Mater.* **1999**, *11*, 1006.
(19) (a) Oldenburg, S. J.; Averitt, R. D.; Westcott, S. L.; Halas, N. J. *Chem. Phys. Lett.* **1998**, *288*, 243. (b) Oldenburg, S. J.; Jackson, J. B.; Westcott, S. L.; Halas, N. J. *Appl. Phys. Lett.* **1999**, *75*, 2897.
(20) Mulvaney, P.; Liz-Marzán, L. M.; Giersig, M.; Ung, T. *J. Mater. Chem.* **2000**, *10*, 1259.
(21) Subramanya Mayya, K.; Gittings, D. I.; Caruso, F. *Chem. Mater.* **2001**, *13*, 3833.

10.1021/cm060403j CCC: $33.50
Published on Web 07/28/2006

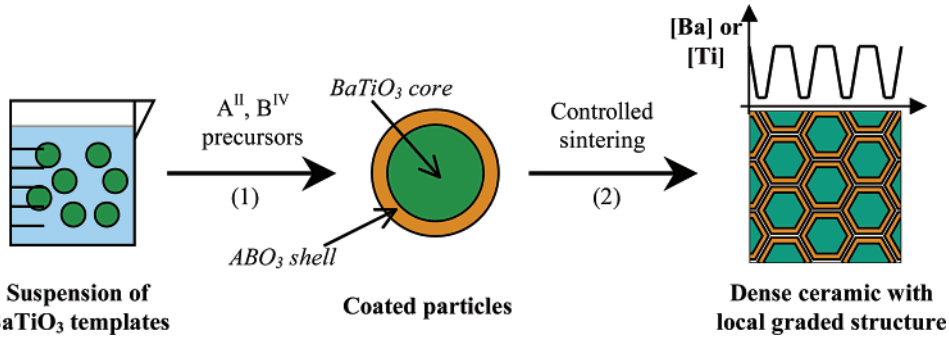

Figure 1. Schematic illustration of the approach for preparing polycrystalline dielectric materials with local graded structure. The first step corresponds to the coating of the $BaTiO_3$ core templates by solution precipitation. The second step corresponds to the controlled sintering of the core−shell particles to a dense ceramic with limited interdiffusion.

can also be considered as building blocks to fabricate dense polycrystalline materials with periodic composition fluctuations. However, the consolidation of core−shell particles in bulk materials by sintering has not been fully explored yet, mainly because of the difficulty of controlling interdiffusion and interface reactions. In this study we describe the coating of $BaTiO_3$ particles with a different ABO_3 perovskite and the sintering of the resulting core−shell particles in dense ceramics, as schematically depicted in Figure 1. This process represents an alternative to the conventional solid-state route for the preparation of dielectric ceramics with inhomogeneous composition. More generally, the same approach can be applied to the preparation of ordered nanocomposites and materials with local graded structure.

Dielectric composites have been recently obtained by sintering of SiO_2-coated (Ba,Sr)TiO_3 particles.[25] In this case densification occurs at relatively low temperatures (≈1000 °C) by viscous flow of the silica glass shell without significant chemical interactions. The composites display very weak dielectric losses but a rather low dielectric constant because of the presence of the continuous silica layer with low permittivity around the ferroelectric grains. In the present case, suitable ABO_3 coating compounds were selected according to the following properties: (i) ABO_3 and $BaTiO_3$ form a solid solution over a broad composition range; (ii) the Curie temperature of the ABO_3−$BaTiO_3$ solid solution is strongly dependent on composition; and (iii) the dielectric constant of the solid solution is high (>1000). Perovskites that fulfill these requiments are, for example, $SrTiO_3$ and $BaZrO_3$. Strontium titanate is an incipient ferroelectric (or quantum paraelectric)[26] in which a polar or ferroelectric phase can be induced at low temperature by isotopic substitution or by substitutional impurities (like Ba and Ca) as well as by an external stress.[26−29] Although $BaZrO_3$ is not ferroelectric, $BaZrO_3$−$BaTiO_3$ solid solutions exhibith ferroelectric behavior up 15 mol % $BaZrO_3$, a diffuse phase transition between 15 and 25 mol %, and a relaxor state at higher concentrations of $BaZrO_3$[30−32] (at least up to 40 mol %). According to Jaffe,[33] both systems display complete solid solubility and possess a high dielectric constant, and the Curie temperature is very sensitive to composition (4−5 °C/mol %). Complete solid solubility between $BaTiO_3$ and $BaZrO_3$ was also reported by Vivekanandan et al.[34] In contrast, Sciau et al.[35] state that the solid solution $BaZr_xTi_{1-x}O_3$ does not exist for $x > 0.42$.

2. Experimental Procedure

Materials. $BaCl_2 \cdot 2H_2O$ (99%), $SrCl_2 \cdot 6H_2O$ (99%), $ZrCl_4$ (99.5%), NH_4OH (28% solution), and NaOH (99%) were supplied by Aldrich. $TiCl_4$ (99.9%) was purchased from Acros Chemical. The water used in the experiments was always freshly distilled water.

Synthesis of $BaTiO_3$ Cores. Synthesis of barium titanate particles was carried out according to the overall formal reaction[36,37]

$$BaCl_2(aq) + TiCl_4(aq) + 6NaOH(aq) \rightarrow BaTiO_3(s) + 6NaCl(aq) + 3H_2O(l) \quad (1)$$

where (aq) denotes a salt in aqueous solution. An acidic $TiOCl_2$ mother solution (3.77 mol/kg) was prepared by drop-by-drop addition of $TiCl_4$ in water cooled in a ice bath. The precise titanium content of this solution was determined by gravimetric titration. For this purpose, the chloride solution was added with excess ammonia, and the precipitate was washed and calcined at 800 °C to obtain a TiO_2 powder. The required amount of the $TiOCl_2$ mother

(22) Salgueiriño-Maceira, V.; Caruso, F.; Liz-Marzán, L. M. *J. Phys. Chem. B* **2003**, *107*, 10990.
(23) Lee, J.-Y.; Lee, J.-H.; Hong, S.-H.; Lee, Y. K.; Choi, J.-Y. *Adv. Mater.* **2003**, *15*, 1655.
(24) Lee, S.-w.; Drwiega, J.; Wu, C.-Y.; Mazyck, D.; Sigmund, W. M. *Chem. Mater.* **2004**, *16*, 1160.
(25) (a) Huber, C.; Treguer-Delapierre, M.; Elissalde, C.; Weill, F.; Maglione, M. *J. Mater. Chem.* **2003**, *13*, 650. (b) Hornebecq, V.; Huber, C.; Maglione, M.; Antonietti, M.; Elissalde, C. *Adv. Funct. Mater.* **2004**, *14*, 899. (c) Mornet, S., Elissalde, C.; Hornebecq, V.; Bidault, O.; Duguet, E.; Brisson, A.; Maglione, M. *Chem. Mater.* **2005**, *17*, 4530.
(26) Müller, K. A.; Burkard, H. *Phys. Rev. B* **1979**, *19*, 3593.
(27) Itoh, M.; Wang, R.; Inaguma, Y.; Yamaguchi, T.; Shan, Y. J.; Nakamura, T. *Phys. Rev. Lett.* **1999**, *82*, 3540.
(28) (a) Bednorz, J. G.; Müller, K. A. *Phys. Rev. Lett.* **1984**, *52*, 2289. (b) Porokhonskyy, V.; Pashkin, A.; Bovtun, V.; Petzelt, J.; Savinov, M.; Samoukhina, P.; Ostapchuk, T.; Pokorny, J.; Avdeev, M.; Kholkin, A.; Vilarinho, P. *Phys Rev. B* **2004**, *69*, 144104. (c) Tkach, A.; Vilarinho, P. M.; Kholkin, A. L. *Appl. Phys. Lett.* **2005**, *86*, 172902.
(29) Haeni, J. H.; Irvin, P.; Chang, W.; Uecker, R.; Reiche, P.; Li, Y. L.; Choudhury, S.; Tian, W.; Hawley, M. E.; Craigo, B.; Tagantsev, A. K.; Pan, X. Q.; Streiffer, S. K.; Chen, L. Q.; Kirchoefer, S. W.; Levy, J.; Schlom, D. G. *Nature* **2004**, *430*, 758.
(30) Hennings, D.; Schnell, A.; Simon, G. *J. Am. Ceram. Soc.* **1982**, *65*, 539.
(31) Dobal, P. S.; Dixit, A.; Katiyar, R. S.; Yu, Z.; Guo, R.; Bhalla, A. S. *J. Appl. Phys.* **2001**, *89*, 8085.
(32) Simon, A.; Ravez, J.; Maglione, M. *J. Phys.: Condens. Matter* **2004**, *16*, 963.
(33) Jaffe, B. *Piezoelectric Ceramics*; Academic Press: London, 1971; p 101.
(34) Vivekanandan, R.; Philip, S.; Kutty, T. R. N. *Mater. Res. Bull.* **1986**, *22*, 99.
(35) Sciau, Ph.; Calvarin, G.; Ravez, J. *Solid State Commun.* **2000**, *113*, 77.

solution was diluted with water in a 500 mL polypropylene vessel, and solid $BaCl_2 \cdot H_2O$ (Aldrich, 99.9%) was added in the amount required to have a [Ba]/[Ti] molar ratio of 1.11. Typically, 250 mL of chloride solution are used. The suspension was stirred until dissolution of the solid chloride. The resulting solution was then quickly mixed (20 s) under vigorous stirring with the same volume of a NaOH (Aldrich, 99%) solution with immediate formation of a gelatinous suspension of titanium hydroxide gel. An excess of NaOH compared to the stoichiometric amount required by reaction 1 was used to guarantee quantitative precipitation of $BaTiO_3$. This excess corresponds to $[OH^-] = 1$ mol dm^{-3} (i.e., a pH of about 14) in the final barium titanate suspension. The vessel was then closed, heated in a thermostatic bath, and kept at a constant temperature of 92 °C under stirring for 1 h. The size of the final $BaTiO_3$ particles is determined by the concentration of the chloride solution:[36,37] particles with a diameter of ≈200 nm were obtained using a titanium concentration (referred to as the chloride solution before addition of NaOH) of 0.2 mol dm^{-3} whereas particles of ≈500 nm were produced at a concentration of 0.09 mol dm^{-3}. After reaction, the $BaTiO_3$ precipitate was separated by centrifugation, washed, and freeze-dried. It is worth noting that the $BaTiO_3$ particles prepared as described above consist of ordered aggregates of primary nanocrystals with a high degree of alignment. Further details on the preparation and properties of the barium titanate templates can be found elsewhere.[36,37]

Coating of $BaTiO_3$ Cores. *$BaTiO_3$@$SrTiO_3$.* An aliquot of the $TiOCl_2$ mother solution is diluted with water to obtain a titanium concentration of ≈1.5 mol dm^{-3}. Solid $SrCl_2 \cdot 6H_2O$ is added to this solution in the amount required to have a Sr/Ti molar ratio of 1.04. The amount of chloride solution used for the coating process is determined by the quantity of $SrTiO_3$ that needs to be precipitated on the $BaTiO_3$ cores. As an example, for the preparation of a coated powder consisting of 20 g of $BaTiO_3$ (64 mol %) and 8.84 g of $SrTiO_3$ (36 mol %), the chloride solution was prepared from 12.77 g of the $TiOCl_2$ mother solution, 13.35 g of $SrCl_2 \cdot 6H_2O$, and 18.7 mL of water. The coating process was carried out in a 250 mL closed Teflon vessel. The closed environment avoids adsorption of CO_2 from air and subsequent formation of carbonates. A concentrated slurry is prepared inside the vessel by suspending 20 g of $BaTiO_3$ core particles in a NaOH solution prepared from 9.37 g of NaOH and 10 mL of water. The amount of NaOH in the slurry is that required to have, after quantitative precipitation of $SrTiO_3$ (assuming a reaction equivalent to reaction 1), $[OH^-] \approx 1$ mol dm^{-3}. The chloride solution was quickly added (10 s) to the suspension under vigorous stirring provided by a magnetic stirrer. The reaction is rather exothermic and produces a sudden temperature increase up to ≈80 °C. Then the vessel was kept for 4 h at 90 °C while stirring inside a thermostatic bath. The temperature of the bath was automatically controlled by a Pt thermoresistance. The suspension was washed with an ammonia solution (pH 12) until chloride ions in the supernatant were no longer detected by precipitation with a $AgNO_3$ solution. Finally the precipitate was collected by filtration and freeze-dried.

$BaTiO_3$@$BaZrO_3$. A $ZrOCl_2$ mother solution with a concentration of 1.3 mol/kg was prepared by dissolving $ZrCl_4$ in water. Solid $BaCl_2 \cdot 2H_2O$ is directly added to this solution without further dilution in the amount required to have a Ba/Zr molar ratio of 1.01. The coating of $BaTiO_3$ with $BaZrO_3$ was carried out using the same methodology described above. As an example, for the preparation of a coated powder consisting of 20 g of $BaTiO_3$ (80 mol %) and 5.93 g of $BaZrO_3$ (20 mol %) the chloride solution was prepared from 16.2 g of the $ZrOCl_2$ mother solution and 5.29 g of $BaCl_2 \cdot 2H_2O$. The $BaTiO_3$ suspension was prepared from 20 g of $BaTiO_3$, 5.65 mL of water, and 4.48 g of NaOH.

Densification. Dense ceramics samples (diameter, 1.2 cm; thickness, 0.1−0.2 cm) were obtained from the $BaTiO_3$@$SrTiO_3$ powders by spark plasma sintering (SPS). The powder was loaded directly into a cylindrical graphite pressure die. The die was then placed inside a SPS furnace (Dr. Sinter 2050, Sumitomo Coal Mining Co., Tokyo, Japan), and the system was evacuated. The sintering conditions were chosen to have a good densification without grain growth. The sample was heated at 200 °C/min up to 1100 °C and held at this temperature for 2 min. The heating was provided by a pulsed direct current current directly flowing through the graphite die. During the entire heating and sintering process a uniaxial constant pressure of 100 MPa was applied. The temperature was recorded by means of a pyrometer focused on a small hole in the graphite die wall. Then the pressure was released, and the sample cooled at ≈400 °C/min. The as-sintered ceramics were polished and then annealed in air for 2 h at 800 °C. This treatment was intended to relieve the residual stresses (arising either from the SPS process or from polishing), remove the surface carbon contamination, and eliminate the oxygen vacancies (and the related electron conduction) possibly produced during SPS treatment by the local reducing conditions imposed by the contact with the graphite die and by the vacuum conditions. Reoxidation at temperatures above 800 °C was not attempted to minimize interdiffusion between the core and the shell regions.

The powders consisting of $BaTiO_3$@$BaZrO_3$ particles were compacted in cylindrical green bodies (diameter, 1 cm) by means of cold isostatic pressing and then sintered in air for 30 min at 1285 °C ($BaZr_{0.2}Ti_{0.8}O_3$) or at 1310 °C ($BaZr_{0.4}Ti_{0.6}O_3$) in a conventional furnace. The heating rate was 5 °C/min.

Homogeneous solid solutions of both systems were obtained by sintering the powders for 6 h in air at 1400−1500 °C. The density of these ceramics was ≈95% of the theoretical X-ray diffraction (XRD) density.

Characterization. To check the effective overall composition of the sintered samples, a series of dense (97−98%) $Sr_xBa_{1-x}TiO_3$ ceramics with different compositions ($x = 0.1, 0.2, 0.3, 0.4, 0.5$) were prepared by conventional solid-state processing using $BaCO_3$, $SrCO_3$, and TiO_2 as raw materials. The permittivity of these ceramics was measured between 220 and 500 K, and the corresponding T_C was determined from the position of the maximum of the permittivity curve. The values of the Curie temperature as a function of the composition x were almost perfectly described by a straight line (squared correlation coefficient 0.999). The regression line was then used to determine the composition of the homogeneous solid solutions obtained by sintering the core−shell $BaTiO_3$@$SrTiO_3$ particles at high temperature. A second calibration curve was obtained from the values of the average lattice parameter, $(a^2c)^{1/3}$ (a and c are the lattice parameters of the tetragonal unit cell), of the $Sr_xBa_{(1-x)}TiO_3$ solid solutions. The overall composition of the $BaTiO_3$@$BaZrO_3$ ceramics was checked by comparing the temperature of the maximum of the permittivity with the data reported in previous studies.[30−32]

The density of the sintered samples was measured by Archimedes' method by immersion in water. In the case of ceramics with nonhomogeneous composition, an estimate of the relative density and of the densification level was obtained by comparing the measured density with the theoretical density of the corresponding homogeneous ceramics determined from the volume of the unit cell. Scanning electron microscopy (SEM) observation was conducted with a LEO1450 VP instrument operated at 15 kV.

(36) Testino, A.; Buscaglia, M. T.; Viviani, M.; Buscaglia, V.; Nanni, P. *J. Am. Ceram. Soc.* **2004**, *87*, 79.
(37) Testino, A.; Buscaglia, M. T.; Buscaglia, V.; Viviani, M.; Bottino, C.; Nanni, P. *Chem. Mater.* **2004**, *16*, 1536.

Transmission electron microscopy (TEM) and electron diffraction (ED) were performed with a JEOL J2010 operated at 200 kV and equipped with a energy-dispersive X-ray analyzer. In both cases, the powder was dispersed in absolute ethanol and a drop of the suspension deposited on a aluminum stub (SEM) or a carbon-coated copper grid (TEM) and dried. XRD patterns were collected with a Philips PW1710 powder diffractometer using the Co Kα radiation (voltage 40 kV, current 30 mA, counting time 10 s/step, range 20−120° 2θ, step scan 0.03° 2θ, secondary graphite monochromator). The powder was poured and pressed in a plastic sample holder. The thickness of the powder bed was 0.2 cm, and the diameter was 2 cm. Lattice parameters were obtained by the Rietveld refinement method and the Cerius^2 software (Molecular Simulations, San Diego, CA), without the use of an internal standard. Measurement of the lattice parameters of reference powders (silicon, corundum) has shown a typical error of ±0.001 Å. Permittivity measurements were performed at a frequency of 1 kHz in the range 20−500 K (heating/cooling rate, 0.5 K min^{-1}) with an applied voltage of 1 V using a Solartron SI1260 impedance analyzer and a ARS closed-vessel type cryostat. For this purpose, gold electrodes were sputtered on the upper and lower surfaces of polished sintered disks.

3. Results and Discussion

3.1. Morphology and Composition of the $BaTiO_3$ Coated Particles. Two different systems, corresponding to $BaTiO_3$ particles coated with either $SrTiO_3$ ($BaTiO_3$@$SrTiO_3$) or $BaZrO_3$ ($BaTiO_3$@$BaZrO_3$), were chosen to explore distinct situations corresponding to partial substitution either of the divalent (Ba) or the tetravalent (Ti) cation. To show the versatility of the coating method, barium titanate cores of two different sizes, ≈200 and ≈500 nm, were used to prepare the $BaTiO_3$@$SrTiO_3$ particles. An example of the initial morphology of the $BaTiO_3$ cores is shown in the inset of Figure 2a. For the $BaTiO_3$@$BaZrO_3$ particles, only the biggest cores were used. The overall composition can be tailored by changing the amount of $SrTiO_3$ or $BaZrO_3$ precipitated from solution. Powders with the following nominal compositions were prepared (the numbers in parentheses define the sizes of the $BaTiO_3$ cores): $Ba_{0.64}Sr_{0.36}TiO_3$ (500 nm), $Ba_{0.44}Sr_{0.56}TiO_3$ (200 nm), $BaZr_{0.2}Ti_{0.8}O_3$ (500 nm), and $BaZr_{0.4}Ti_{0.6}0_3$ (500 nm). The effective overall compositions of the homogeneous $Ba_{1-x}Sr_xTiO_3$ ceramics prepared from the $BaTiO_3$@$SrTiO_3$ powders, estimated as described before, were $x = 0.34$ and $x = 0.55$, respectively. The difference between nominal and effective compositions can be considered within the experimental error, meaning that there was not a significant loss of $SrTiO_3$ during the washing process. It is worth noting that the use of the T_C data reported by Jaffe[33] for $Sr_xBa_{1-x}TiO_3$ solid solutions leads to a systematic underestimation of the $SrTiO_3$ content in the ceramic. For the homogeneous ceramics prepared from the $BaTiO_3$@$BaZrO_3$ powders the temperature of the maximum of the permittivity was in good agreement (±5 °C) with the values reported[30−32] for the nominal compositions. Thus the difference between effective and nominal composition is within ±1 mol %.

Direct evidence of the growth of a shell of the second perovskite on the suspended $BaTiO_3$ particles is provided by SEM, as shown in Figure 2a,b. TEM has revealed, in the case of $BaTiO_3$@$SrTiO_3$ particles, a granular coating composed of faceted $SrTiO_3$ nanocrystals of ≈10 nm (Figure 2c,d). Observation in high resolution and ED show that most of the $SrTiO_3$ nanocrystals in the coating layer are randomly oriented. The deposition of $BaZrO_3$ (Figure 2b,e) leads to more homogeneous and compact coatings comprised of $BaZrO_3$ rounded nanocrystals of ≈10 nm (Figure 2e,f). In contrast to the $SrTiO_3$ coating, the $BaZrO_3$ crystallites are preferentially aligned along a few crystallographic directions and present a well-defined orientation with the substrate, as in hetero-epitaxial growth. Further evidence of the presence of a coating was given by energy-dispersive X-ray analysis which revealed the presence of Sr(Zr) at the surface of the particles. XRD patterns of the as-prepared core−shell particles are shown in Figure 3 (bottom traces). Comparison with the diffraction patterns of the $BaTiO_3$ templates and of $SrTiO_3$ and $BaZrO_3$ nanopowders precipitated in the same experimental conditions adopted for the coating process (see Supporting Information, Figures S1 and S2) shows that the spectra of the coated powders correspond to the superposition of the patterns of two perovskites and other phases were not detected.

Colloidal oxide particles dispersed in aqueous solution at high pH show a strongly negative zeta potential.[38] However, in the experimental conditions adopted for the coating process, the electrostatic repulsive barrier, is expected to be completely suppressed due to the high ionic strength of the solution. Consequently, the interactions between the $BaTiO_3$ particles and the $SrTiO_3$/$BaZrO_3$ nanocrystals generated during the reaction are of the attractive type. This produces the coagulation of the nanoparticles on the cores. The macroscopic driving force responsible for the spontaneous assembly of the nanocrystals in the shell is related to the replacement of solid−liquid interfaces by solid−solid interfaces of lower energy and to the entropy increase resulting from the removal of water and/or adsorbed ions. In the case of the highly oriented attachment ($BaTiO_3$@$BaZrO_3$), the energy gain is even larger because of the creation of quasi-coherent interfaces. The less dense and more irregular coating obtained with $SrTiO_3$ probably indicates that some nanoparticle aggregation occurs before the particles attach on the core surface, leading to the observed disordered shell structure.

Compared to other techniques, the proposed coating route does not require the use of organic solvents and employs relatively inexpensive inorganic precursors, like chlorides. Because the perovskite shell directly grows from solution, the separate preparation of preformed nanoparticles to be adsorbed on the template cores is not required. A further advantage is that $BaTiO_3$ core particles primarily define the size distribution of the coated colloids and, after sintering, the grain size of the final ceramic, as will be shown later. Therefore, the $BaTiO_3$ particles not only determine the functional properties of the material but also act as a template for the development of the final microstructure. Finally, the

(38) (a) Bae, H. S.; Lee, M. K.; Kim, W. W.; Rhee, C. K. *Colloids Surf., A* **2003**, *220*, 169. (b) Blanco-Lopez, M. C.; Rand, B.; Riley, F. L. *J. Eur. Ceram. Soc.* **1997**, *17*, 281. (c) Paik, U.; Hackley, V. A. *J. Am. Ceram. Soc.* **2000**, *83*, 2381. (d) Shen, Z.-G.; Chen, J.-F.; Zou, H.-k.; Yun, J. *J. Colloid Interface Sci.* **2004**, 275, 158. (e) Nadkarni, S. S.; Smay, J. E. *J. Am. Ceram. Soc.* **2006**, *89*, 96.

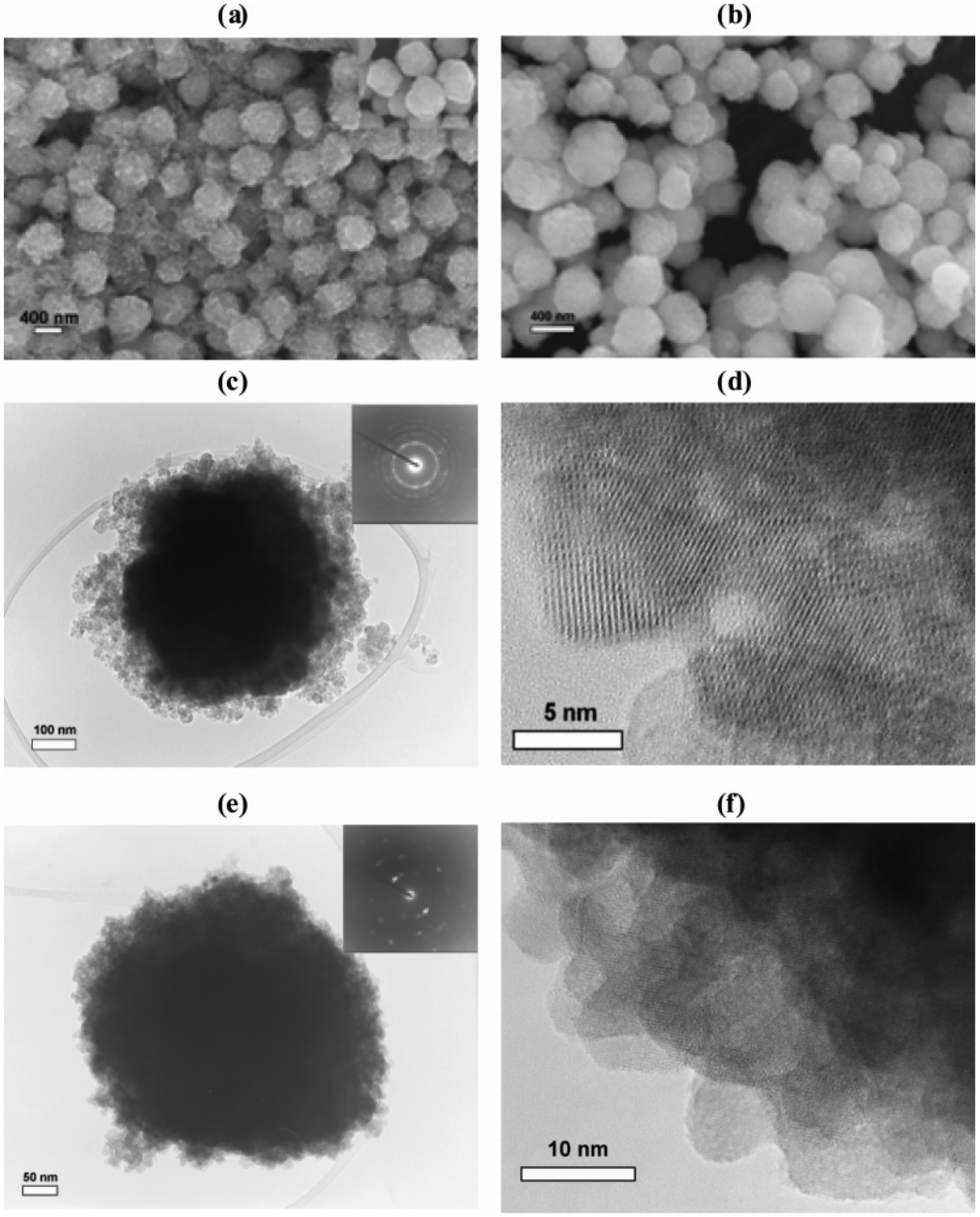

Figure 2. Morphology of $BaTiO_3$ core−shell particles. (a) $BaTiO_3$@$SrTiO_3$. The inset shows template $BaTiO_3$ particles before coating. (b) $BaTiO_3$@$BaZrO_3$. (c) TEM image of a typical $BaTiO_3$@$SrTiO_3$ particle. (d) High-resolution TEM image of $SrTiO_3$ nanocrystals of the shell. (e) TEM image of a typical $BaTiO_3$@$BaZrO_3$ particle; (f) High-resolution TEM image of the nanocrystalline $BaZrO_3$ coating. The ED patterns shown in the insets of parts c and e reveal different structures of the coating layers. The orientation of the $SrTiO_3$ nanocrystals is almost random, whereas certain preferential orientations are observed for the $BaZrO_3$ nanocrystals as also apparent from part f.

aqueous chemistry involved in the process should facilitate the preparation of a series of core−shell perovskite particles, where the divalent element can be Ca, Sr, Ba, and Pb and the tetravalent element can be Ti, Zr, Sn, and Hf. The thermodynamic modeling work of Riman and co-workers[39] has shown that alkaline-earth titanates and zirconates can be synthesized in aqueous solution even at temperatures below 100 °C provided that the pH is high enough. The main drawbacks of the described coating process are inherent to the exothermicity of the reaction and the use of a highly concentrated slurry of $BaTiO_3$ which make difficult the scale-up and the production of large amounts of core−shell particles. However, the goal of this study is rather to show the feasibility of obtaining ceramic materials with local graded structure by controlled sintering of coated particles than to propose a convenient synthesis route for mass production of core−shell colloids.

3.2. Microstructure and Composition of the Sintered Ceramics. Attempts to consolidate $BaTiO_3$@$SrTiO_3$ particles in dense ceramics by conventional sintering resulted in the formation of rather homogeneous solid solutions. This is ascribed to a relatively fast interdiffusion of Ba and Sr in the perovskite lattice. In contrast, densification with limited interdiffusion was obtained by SPS. This process enables a

(39) (a) Lencka, M. M.; Riman, R. E. *Chem. Mater.* **1993**, *5*, 61. (b) Lencka, M. M.; Riman, R. E. *J. Am. Ceram. Soc.* **1993**, *76*, 2649. (c) Lencka, M. M.; Riman, R. E. *Chem. Mater.* **1995**, *7*, 18. (d) Lencka, M. M.; Nielsen, E.; Anderko, A.; Riman, R. E. *Chem. Mater.* **1997**, *9*, 1116.

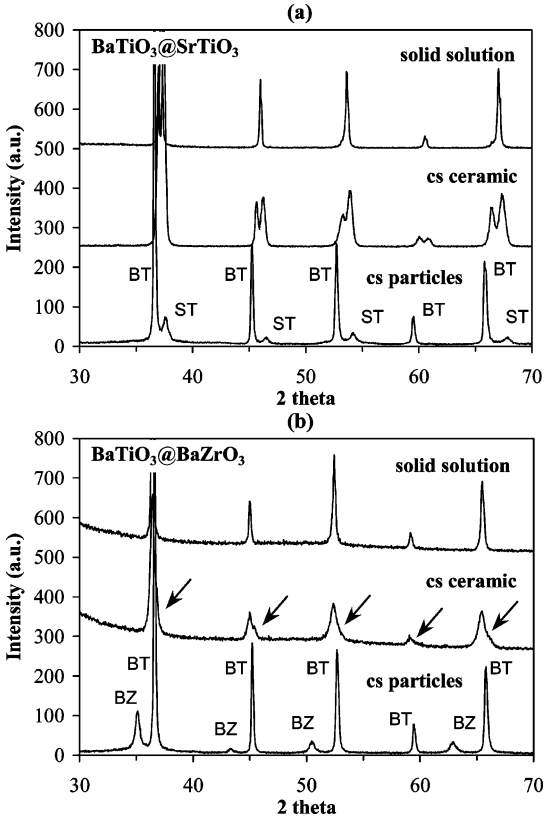

Figure 3. XRD patterns of core−shell $BaTiO_3$ powders and corresponding ceramics. (a) $Ba_{0.66}Sr_{0.34}TiO_3$. XRD patterns of as-prepared coated particles (bottom), sintered material with core−shell grains (center), and homogeneous solid solution (top). (b) $BaZr_{0.2}Ti_{0.8}O_3$. XRD patterns of as-prepared coated particles (bottom), sintered material with core−shell grains (center), and homogeneous solid solution (top). The growing background below 40° 2θ comes from the plastic sample holder. The arrows indicate the shoulder on the high-angle side of the peaks ascribed to the $BaTiO_3$-rich core. BT, $BaTiO_3$; ST, $SrTiO_3$; BZ, $BaZrO_3$.

powder compact to be sintered to high density at relatively low temperatures and in a short time, typically a few minutes, in comparison to conventional sintering. The ability of SPS to produce dense and fine grained polycrystalline materials, nanocrystalline ceramics, laminated structures, and even composites containing metastable or nonequilibrium phases has been demonstrated for a broad variety of systems.[40−45] Thus, SPS is particularly suitable for the consolidation of core−shell particles when diffusion of the coating species is rapid. The final density of the $BaTiO_3$@$SrTiO_3$ ceramics was ≈97% of the theoretical density of the corresponding homogeneous ceramics. SEM observation on fracture or thermally etched surfaces shows a dense homogeneous microstructure with grain size close to the diameter of the starting particles (Figure 4). Thermal etching (Figure 4b)

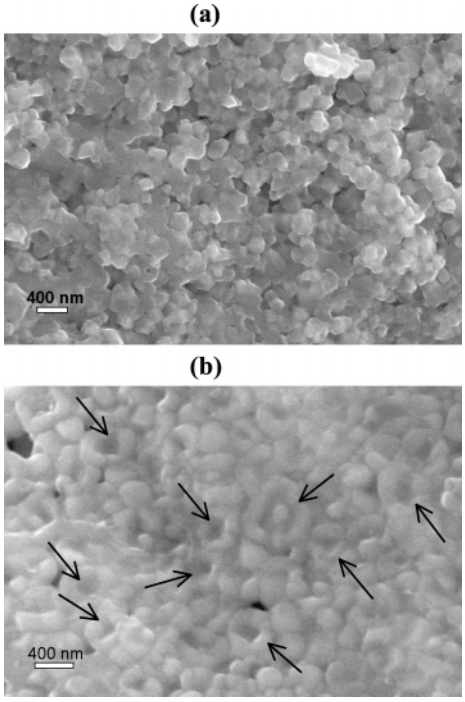

Figure 4. Microstructure of ceramics with local graded structure obtained by sintering $BaTiO_3$@$SrTiO_3$ core−shell particles. (a) Fracture surface of a ceramic with overall composition $Ba_{0.45}Sr_{0.55}TiO_3$ (diameter of the initial $BaTiO_3$ cores, ≈200 nm). (b) Polished and thermally etched surface of a ceramic with overall composition $Ba_{0.66}Sr_{0.34}TiO_3$ (diameter of the initial $BaTiO_3$ cores, ≈500 nm). The arrows indicate the grains in which a core−shell structure is more evident. Bar: 400 nm.

produces a peculiar morphology corresponding to the formation of a depression at the center of the grains probably originated from the core−shell structure of the grains. This inhomogeneous structure is more evident in backscatter electron images (atomic number contrast) of polished surfaces (Figure 5). A nonhomogeneous, concentric distribution of Sr and Ba is clearly observed for most of the grains of the ceramic (Figure 5a). The darker phase in Figure 5a corresponds to a $SrTiO_3$-enriched shell which forms a continuous network in the microstructure. A similar microstructure was also detected in the ceramic with overall composition $Ba_{0.45}Sr_{0.55}TiO_3$ although the observation was more difficult because of the smaller size of the grains. XRD spectra of the sintered samples with core−shell grains correspond to the superposition of two different patterns, that is, a $BaTiO_3$-rich phase and a $SrTiO_3$-enriched phase, respectively (see Figure 3a, center trace, and Supporting Information, Figure S3). The peaks of both phases appear significantly broadened in comparison to the homogeneous solid solution, indicating the existence of a composition gradient. These results provide a further confirmation of the existence of a core−shell structure in the sintered material. A variation of the relative intensities of the two components with respect to the as-coated powder can be noticed. This originates from the partial interdiffusion between core and shell, which leads to the formation of a $SrTiO_3$-enriched phase in the grain boundary region, while the cores of the grains correspond to a $BaTiO_3$-rich phase. The small volume variations originated by the interdiffusion process can lead also to development of stresses inside the grains and additional strain broadening of the XRD peaks. A further

(40) Nygren, M.; Shen, Z. *Solid State Sci.* **2003**, *5*, 125.
(41) Shen, Z.; Adolfsson, E.; Nygren, M.; Gao, L.; Kawaoka, H.; Niihara, K. *Adv. Mater*. **2001**, *13*, 214.
(42) Shen, Z.; Zhao, Z.; Peng, H.; Nygren, M. *Nature* **2002**, *417*, 266.
(43) (a) Zhao, Z.; Buscaglia, V.; Viviani, M.; Buscaglia, M. T.; Mitoseriu, L.; Testino, A.; Nygren, M.; Johnsson, M.; Nanni, P. *Phys. Rev. B* **2004**, *70*, 024107. (b) Buscaglia, M. T.; Viviani, M.; Buscaglia, V.; Mitoseriu, L.; Testino, A.; Nanni, P.; Zhao, Z.; Nygren, M.; Harnagea, C.; Piazza, D.; Galassi, C. *Phys Rev. B* **2006**, *73*, 064114.
(44) (a) Anselmi-Tamburini, U.; Garay, J. E.; Munir, Z. A.; Tacca, A.; Maglia, F.; Spinolo, G. *J. Mater. Res.* **2004**, *19*, 3255. (b) Anselmi-Tamburini, U.; Garay, J. E.; Munir, Z. A. *Scr. Mater.* **2006**, *54*, 823.
(45) Shen, Z.; Liu, J.; Grins, J.; Nygren, M.; Wang, P.; Kan, Y.; Yan, H.; Sutter, U. *Adv. Mater.* **2005**, *17*, 676.

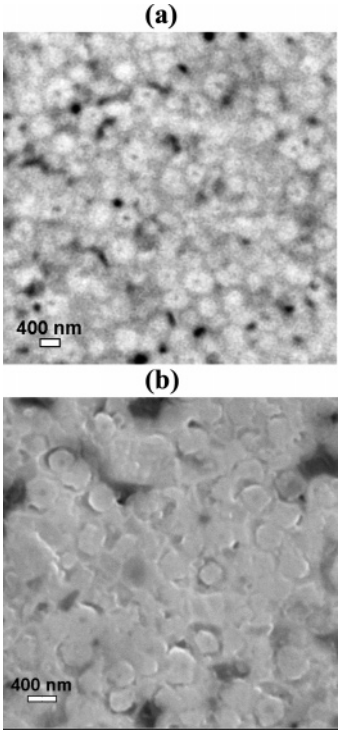

Figure 5. Microstructure of ceramics with local graded structure obtained by sintering $BaTiO_3$ core−shell particles. (a) Backscatter electron image of the polished surface of a $BaTiO_3$@$SrTiO_3$ ceramic (densified for 2 min at 1100 °C by SPS, overall composition $Ba_{0.66}Sr_{0.34}TiO_3$, diameter of the initial $BaTiO_3$ cores ≈ 500 nm) revealing a concentric, nonuniform distribution of Sr and Ba. (b) Etched polished surface of a $BaTiO_3$@$BaZrO_3$ ceramic (densified for 30 min at 1285 °C by conventional sintering, overall composition $BaZr_{0.2}Ti_{0.8}O_3$, diameter of the initial $BaTiO_3$ cores ≈ 500 nm) showing the core−shell structure of the grains. Bar: 400 nm.

consequence of the solid-state interdiffusion process is the appearance of a small pore at the center of the grains of the ceramic (Figure 5a), very likely a manifestation of the Kirkendall effect related to different migration rates of Sr and Ba in the perovskite lattice. According to the results of interdiffusion experiments in $BaTiO_3$−$SrTiO_3$ diffusion couples, diffusion of barium in strontium titanate is faster than diffusion of strontium in barium titanate.[46]

In the case of $BaTiO_3$@$BaZrO_3$ particles, good densification of the ceramics (relative density: ≈93% for $BaZr_{0.2}Ti_{0.8}O_3$ and ≈91% for $BaZr_{0.4}Ti_{0.6}O_3$) with partial interdiffusion was obtained by conventional sintering in air at 1285−1310 °C. This indicates a slower migration of Zr and Ti in the perovskite structure in comparison to diffusion of the alkaline-earth cations. Although sintering at higher temperatures produces ceramics with lower porosity, the resulting materials are more homogeneous and display more conventional dielectric properties. Appropriate chemical etching of the polished surface of the final ceramic gives direct evidence of the core−shell microstructure, as shown in Figure 5b. The grain size of the ceramic compares well with the diameter of the starting $BaTiO_3$@$BaZrO_3$ particles, meaning that no appreciable grain growth occurred during sintering. The XRD spectrum of the sintered ceramics again corresponds to the superposition of the patterns of the $BaTiO_3$-rich core and a $BaZrO_3$ enriched shell which merge in broad and asymmetric

(46) Butler, E. P.; Jain, H.; Smyth, D. M. *Diffus. Defect Data, Pt. A* **1989**, *66−69*, 1519.

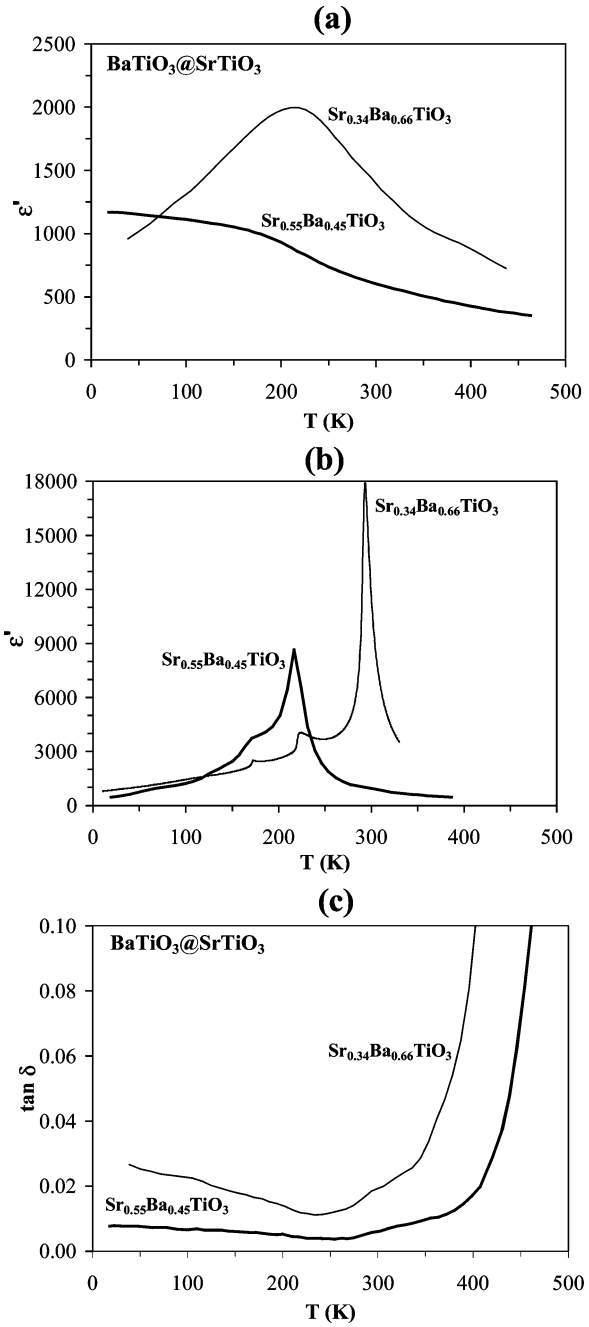

Figure 6. Dielectric properties of ceramics (overall composition $Ba_{0.45}Sr_{0.55}TiO_3$ and $Ba_{0.66}Sr_{0.34}TiO_3$) with local graded structure obtained by sintering $BaTiO_3$@$SrTiO_3$ core−shell particles. (a) Relative dielectric constant. (b) Relative dielectric constant of corresponding homogeneous solid solutions. (c) tan δ.

peaks (Figure 3b, center trace). The evident shoulder on the high 2θ angle side of the XRD peaks can be ascribed to the remnant $BaTiO_3$-rich core and indicates that only partial interdiffusion has occurred.

In summary, SEM images and XRD patterns provide evidence that controlled sintering of $BaTiO_3$ particles coated with either $SrTiO_3$ or $BaZrO_3$ can produce ceramics with grains showing a radial composition gradient (core−shell structure).

3.3. Dielectric Properties. The dielectric properties of the ceramics with core−shell grains were compared (Figures 6 and 7) to those of homogeneous solid solutions obtained from the same powders. XRD patterns (Figure 3, top traces) show

no significant compositional gradients after 6 h of sintering at 1400−1500 °C for both systems. The relative dielectric constant (ϵ') of the homogeneous $Ba_{1-x}Sr_xTiO_3$ solid solutions (Figure 6b) shows a pronounced maximum at the Curie temperature, 217 K for $Ba_{0.45}Sr_{0.55}TiO_3$ and 295 K for $Ba_{0.66}Sr_{0.34}TiO_3$. Further anomalies at lower temperatures correspond to the orthorhomic/tetragonal and the rhombohedral/orthorhombic transitions. In contrast, a continuous decrease of ϵ' with increasing temperature, from ≈1200 at 20 K down to ≈500 at 400 K, is observed for the ceramic $Ba_{0.55}Sr_{0.45}TiO_3$ with core−shell grains (Figure 6a). This means that the shell region still contains a significant amount of pure or almost pure $SrTiO_3$. The Ba-richer $Ba_{0.64}Sr_{0.34}TiO_3$ sample shows, instead, a strongly broadened permittivity peak centered at ≈220 K with a shoulder at ≈400 K corresponding to the existence of a remnant core of pure $BaTiO_3$ (the T_C of barium titanate is ≈398 K).

The dielectric losses (tan δ) of the ceramic $Ba_{0.55}Sr_{0.45}TiO_3$ with core−shell grains are ≤1% between 20 and 370 K (Figure 6c). For $Ba_{0.66}Sr_{0.34}TiO_3$ the losses are higher, although below 3% up to 350 K. The value of tan δ rapidly increases for both samples above 400−450 K. This anomalous increase is not observed in the case of homogeneous solid solutions sintered in air. It is well-known that sintering of $BaTiO_3$ in a reducing atmosphere results in oxygen loss with formation of doubly charged oxygen vacancies electrically compensated by conduction electrons[47] and strong increases of tan δ. Therefore, the ceramics produced by SPS were reoxidized at 800 °C in air (see the experimental section) to improve the dielectric properties. However, the reoxidizing treatment could not have been completely effective because of the relatively large grain size. If the cores of the grains were still slightly conductive, this would explain the high losses above 400 K.

The variation of ϵ' with temperature in the core−shell ceramics is determined by the shape of the concentration profile across the single grains and by the modification of the relative dielectric constant at T_C with composition. In particular, the permittivity of $SrTiO_3$ increases with decreasing temperature and takes rather high values ($>10^4$) below 40 K. In addition, considering the diameter of the starting $BaTiO_3$ cores, a size effect on permittivity cannot be neglected. In a recent investigation[43] it has been shown that there is progressive broadening and flattening of the ϵ' peak when the grain size of $BaTiO_3$ ceramics is reduced below 1 μm. However, this effect becomes important only when the grain size is <300 nm and is accompanied by a strong depression of the dielectric constant. Thus, the size effect should only have a minor effect of the dielectric properties of the nonhomogeneous ceramics obtained from the bigger (500 nm) cores. In contrast, the size effect is probably responsible for the lower permittivity of the $Sr_{0.55}Ba_{0.45}TiO_3$ ceramics with core−shell grains prepared from the smaller (200 nm) $BaTiO_3$ cores. This interpretation is also supported by the results of Liu et al.[48] They have measured the permittivity of $Ba_{0.6}Sr_{0.4}TiO_3$ ceramics with different grain sizes obtained by SPS. It turned out that the maximum permittivity (at 10 kHz) in ceramics with a grain size of 100−200 nm is of the order of 1000, to be compared with values of 5000−6000 found for coarse ceramics with grains of 5−10 μm.

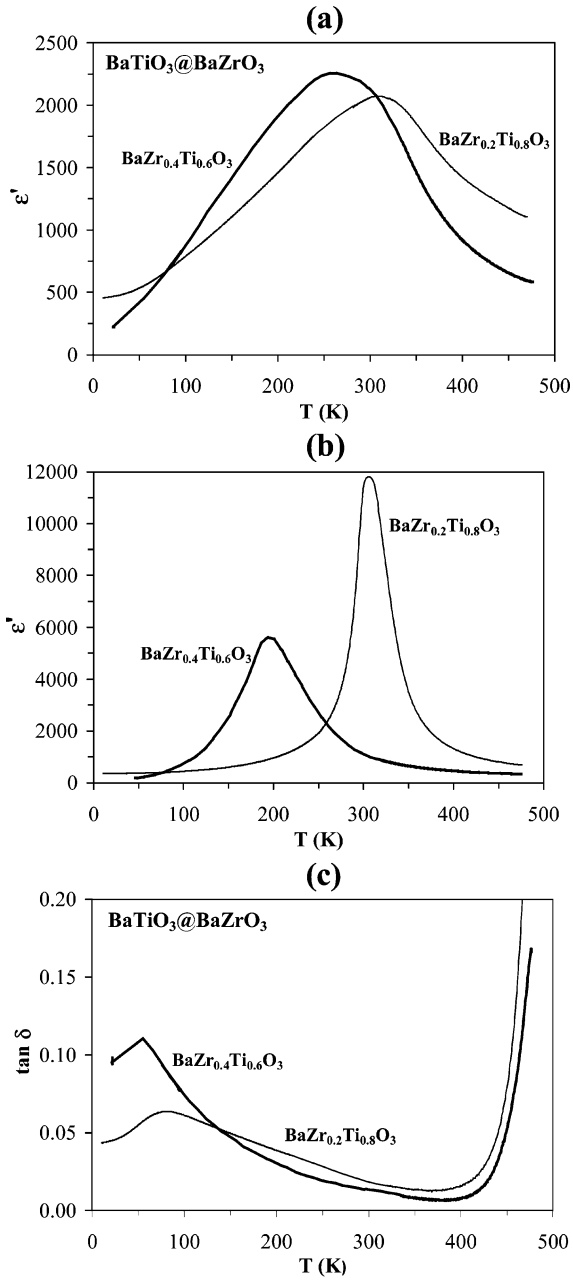

Figure 7. Dielectric properties of ceramics (overall compositions $BaZr_{0.4}Ti_{0.6}O_3$ and $BaZr_{0.2}Ti_{0.8}O_3$) with local graded structure obtained by sintering $BaTiO_3$@$BaZrO_3$ core−shell particles. (a) Relative dielectric constant. (b) Relative dielectric constant of corresponding homogeneous solid solutions. (c) tan δ.

The dielectric constant of $BaTiO_3$@$BaZrO_3$ ceramics with overall compositions $BaZr_{0.2}Ti_{0.8}O_3$ and $BaZr_{0.4}Ti_{0.6}O_3$ is shown in Figure 7a. In comparison to the corresponding $BaZr_xTi_{1-x}O_3$ homogeneous solid solutions (Figure 7b), the ceramic with core−shell grains show a very broadened and flattened permittivity peak. For the composition $x = 0.2$ the permittivity peak is centered at ≈310 K for both the

(47) Chan, N.-H.; Sharma, R. K.; Smyth, D. M. *J. Am. Ceram. Soc.* **1981**, *64*, 556.

(48) Liu, J.; Shen, Z.; Nygren, M. *Ferroelectrics* **2005**, *319*, 335.

inhomogeneous and homogeneous ceramics. The decrease of ϵ' in the range 200−400 K is only of ≈25% in comparison to its maximum value, and tan δ (Figure 7c) is below 4%. The position of the permittivity maximum in the core−shell ceramic $BaZr_{0.4}Ti_{0.6}O_3$ is shifted at a much higher temperature (≈265 K) than the corresponding solid solution (194 K). This shift is explained by the significant decrease of the peak permittivity for solid solutions containing more than 10 mol % $BaZrO_3$.[30−32] The temperature dependence of permittivity is very similar to that of $BaZr_{0.2}Ti_{0.8}O_3$.

4. Conclusions

The controlled sintering of $BaTiO_3$ particles, coated with a different perovskite ($SrTiO_3$, $BaZrO_3$) by means of a precipitation process, represents a novel approach to the fabrication of dense bulk dielectric materials with a locally graded (core−shell) structure. Good densification without significant grain growth and only a limited interdiffusion between core and shell regions can be obtained by a careful optimization of the sintering conditions and, in the case of $BaTiO_3$@$SrTiO_3$ particles, by using the SPS process. In the absence of grain growth, the final microstructure of the ceramic is determined by the size of starting $BaTiO_3$ cores. For both investigated systems, the observed dielectric behavior strongly supports the existence of a radial composition gradient inside the grains related to the core−shell structure of the coated particles. The overall results of this investigation indicate that the relative dielectric constant can be readily modulated by varying the size of the core particles and the relative amount of coating material (i.e., varying the overall composition of the material).

The above features make possible an effective engineering and design of the final material. The proposed method may provide a new avenue for fabricating a wide variety of polycrystalline functional and structural inorganic materials with improved/modulated properties.

Supporting Information Available: XRD patterns (Co Kα radiation) of different powders (Figures S1 and S2) and of a ceramic with local graded structure (Figure S3; PDF). This material is available free of charge via the Internet at http://pubs.acs.org.

CM060403J